Investigation of membrane degradation in polymer electrolyte fuel cells using local gas permeation analysis

Stefan Kreitmeier, Gabriel A. Schuler [1], Alexander Wokaun, Felix N. Büchi*

Electrochemistry Laboratory, Paul Scherrer Institut, CH-5232 Villigen PSI, Switzerland

ARTICLE INFO

ABSTRACT

The effect of chemical and mechanical membrane degradation on the gas separation is investigated in the early stage. The aim is to identify the trigger processes which lead to a nonuniform degradation. Chemical and mechanical degradation are investigated in accelerated stress tests at OCV, relative humidity cycling and a combination of both. Using a tracer gas concept, gas permeation in perfluorosulfonic acid membranes (Nafion) is analyzed locally and online in terms of diffusive and convective gas transport. Local phenomena, such as humidity fluctuations, cracks in the micro porous layer and carbon fibers, are found to initiate the degradation of the gas separation. Pinhole formation, induced by mechanical degradation processes, is crucial for the onset of a synergetic effect. Combined chemical and mechanical degradation accelerates pinhole growth, which is the major source of the increasing gas permeation in Nafion membranes with stabilized end-groups. The spatial nonuniformities of the relative humidity and humidity fluctuations are the main source of inhomogeneous membrane degradation.

1. Introduction

Cost and the durability still limit the commercial use of polymer electrolyte fuel cells (PEFC) for the application in the transport sector [1,2]. The catalyst, its support and the polymer electrolyte membrane are the most susceptible components for failures [3–10]. In the past 40 years perfluorosulfonic acid (PFSA) polymers have been established as the standard material for PEFC membranes, and their degradation under fuel cell conditions has been studied widely [5,6,8,9,11]. Besides proton transport and electric insulation, gas separation is a major function of the membrane in the PEFC. A loss of the gas separation may lead to a sudden death of the fuel cell forcing an immediate shutdown of the system [12]. Therefore, gas permeability is often used as an indicator for degradation. Three different mechanisms degrading the gas separation of the membrane are proposed in the literature. Unzipping of polymer chains by radical attack is referred to as *chemical* degradation. Free hydroxy and hydroperoxy radicals are formed by reactants permeating to the opposite side or by intermediates of the oxygen reduction reaction during fuel cell operation [8,9,13,14]. Membrane creeping, crack and pinhole formation induced by temperature and humidity fluctuations are considered *mechanical* degradation [7,15]. Finally, *thermal* decomposition of the polymer can degrade PFSA membranes if the temperature exceeds locally 200 °C [6,16–18], which may be possible for membranes with pinhole defects [19]. The three degradation mechanisms or a combination thereof can cause membrane thinning and/or pinhole formation, which both degrade the membrane gas separation properties [5,12].

Gas can permeate through membranes by three different transport mechanisms: molecular diffusion, Knudsen diffusion and viscous flow. The gas transport is a function of the pore size as shown in Fig. 1. In the solid and liquid phases of the membrane the gas diffuses by a solution − diffusion process [5]. In free volumes and pores in the range of $d_{molecule} < d_{pores} < \lambda_{mean}$, where $d_{molecule}$ is the molecule diameter, d_{pore} the pore diameter and λ_{mean} the mean free path of the molecule, Knudsen diffusion is the major gas transport mechanism, which may occur in dry hydrophilic clusters formed by sulfonic acid groups [16]. The upper limit of the Knudsen regime is indistinct (blue domains in Fig. 1), since λ_{mean} depends on the gas species, temperature and pressure. Driving force for diffusive gas permeation is the partial pressure difference of the gas species between the two sides of the membrane. When the membrane contains pores, larger than about 0.5 μm and open to both sides of the membrane (pinholes), viscous flow (yellow

* Corresponding author. Tel.: +41 56 310 2411; fax: +41 56 310 4415.
  E-mail address: felix.buechi@psi.ch (F.N. Büchi).
[1] Present address: ABB Corporate Research, Segelhofstrasse 1K, CH-5405 Baden-Dättwil, Switzerland.
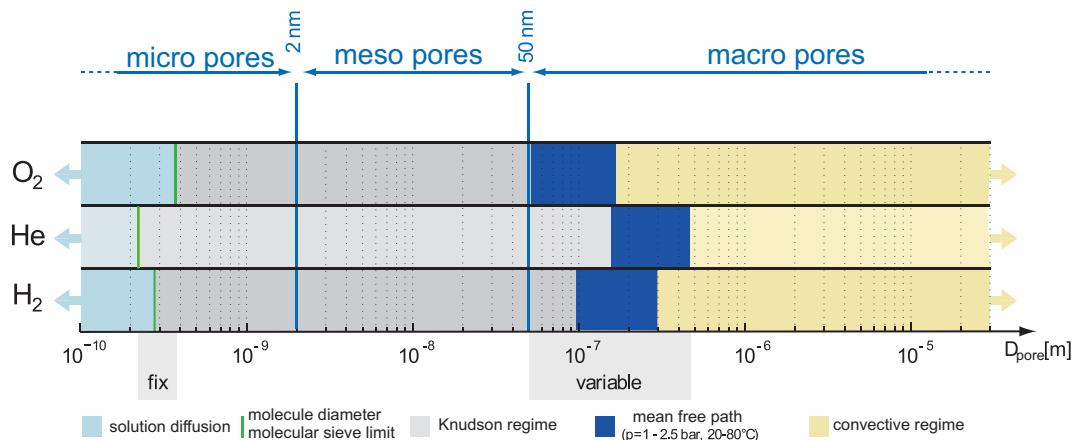
Fig. 1. Gas transport regimes through (porous) membranes are shown for oxygen, helium and hydrogen as a function of the pore size.

domain in Fig. 1) is the dominant gas transport, which is driven by the total pressure difference between the two sides. This process, different from the diffusive gas transport mechanisms, is referred to as convective gas transport.

The gas permeability, often measured electrochemically in terms of the integral hydrogen crossover, is generally the sum of all gas transport mechanisms. However, the diffusive and convective gas transport can be distinguished when analyzing the partial pressure and total pressure driven gas permeations. Therefrom, membrane thinning and pinhole formation can be discriminated by increased diffusive or convective gas crossover, respectively. Degradation processes may have distinct effects on these gas transport mechanisms, which can also be locally different. Parameters influencing membrane degradation, such as reactant composition, relative humidity and temperature, vary across the active area of a fuel cell of technical size. Hence, analysis methods with spatial resolution are required for accurate measurements and interpretation of changes in the gas separation properties of the membrane.

However, only little is known about the spatial distribution of membrane degradation in the literature. Sompalli et al. [22] investigated membrane failures at catalyst layer edges. When the cathode catalyst layer extends over the anode catalyst layer in a membrane electrode assembly (MEA), the potential increases to open circuit voltage (OCV) in the overlap region. This was found to enhance chemical degradation of the membrane in the overlap region. Serincan et al. [23] modeled the stress distribution in the membrane induced by a nonuniform membrane hydration. Parameters such as the relative humidity of the inlet gases, the relative humidity gradient between anode and cathode, the rib/channel geometry and the current density affect the water content of the membrane locally. The inhomogeneity of the membrane hydration causes mechanical stress, which can result in nonuniform mechanical membrane degradation, such as plastic deformation. Stumper et al. [24] used localized polarization curves in combination with OCV profile measurements to calculate local crossover leaks in each cell of a 10-cell stack. They observed that leaks are formed predominately at the gas inlets. They also demonstrated that the total leakage rate can be further deconvoluted into electrical shorts, diffusive and convective components by a systematic variation of operating variables. However, the application to the single cell level is missing.

In this work the effect of chemical and mechanical degradation on the gas separation of the membrane is investigated locally in the early stage in order to identify trigger processes resulting in nonuniform degradation. The results shall ascertain the root cause of the degradation and improve the understanding of membrane degradation mechanisms. Adequate accelerated stress tests (AST) focusing on chemical or mechanical membrane degradation and on their combination are employed. To test the influence of the gas diffusion electrode (GDE) surface structure, two different types of MEAs are assembled with GDEs of different surface roughness. The gas permeation is analyzed by diffusive and convective gas transport to distinguish between membrane thinning and pinhole formation. X-ray tomographic microscopy (XTM), scanning electron microscopy (SEM) and *in situ* analysis of the local water vapor fraction are performed to complete the findings of the gas permeation analysis.

2. Methodology, components and experimental details

2.1. Methodology

Gas transport through the MEA is analyzed by adding helium (10 vol.%) as a tracer to the anode stream, and its permeate concentration is measured locally in the cathode stream using a quadrupole mass spectrometer. The measured gas crossover is denoted as crossover through the membrane in the following, since the gas permeability of the GDE is several orders of magnitude higher than for the membrane in the absence of liquid water and for moderate convective gas permeation [16]. By systematically changing the pressure difference between anode and cathode, gas diffusion through the membrane can be distinguished from the convective gas transport through pinholes [16]. Fig. 2 shows the two transport mechanisms at constant cathode pressure (150 kPa) and different anode pressure levels. At higher anode pressure (160 kPa) helium permeates to the cathode by diffusive and also by convective transport if there are pinholes in the membrane (configuration A). At lower anode pressure (140 kPa) only the diffusive transport takes place even in the presence of pinholes (configuration B). The convective transport of helium from the cathode back to the anode is neglected, as the concentration at the cathode is very low ($\leq$500 ppm). Likewise, the dilution of helium on the anode by permeated nitrogen and oxygen is neglected, since the helium concentration is about 100 times higher at the anode than the measured nitrogen and oxygen concentration (100–1000 ppm). The nitrogen and oxygen concentration may be significantly higher very close to defects, but the spatial resolution of the gas permeation analysis hardware is too low to be affected by this.
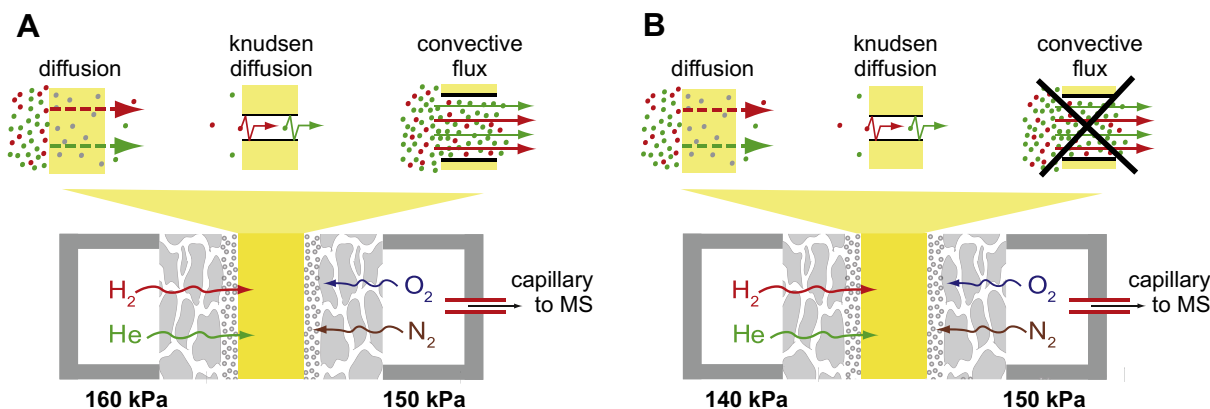
Fig. 2. Concept for distinguishing between diffusive and convective gas permeation in the membrane. A) A higher pressure at the anode induces convective and diffusive helium transport. B) A lower pressure at the anode only allows for diffusive helium transport.

Fig. 3 shows the applied methodology for a new membrane. The helium concentration is measured locally in the center channel of the cathode at an anode pressure of 140 and 160 kPa (Fig. 3A). The helium permeate flux is calculated according to equation (1), where $\dot{V}_{He}$ is the helium permeate flux (ml s^{-1} m^{-2}), c_{He} (vol.%) and c_{N_2} (vol.%) are the measured helium and nitrogen concentrations along the channel, c_{He}^o (vol.%) and $c_{N_2}^o$ (vol.%) are the measured helium and nitrogen concentrations at the anode and cathode inlets, respectively, $\dot{V}$ (ml s^{-1}) is the flow rate of the cathode mass flow controller and A (m^2) is the active cell area. Due to the humidification c_{He}^o is smaller than the applied 10 vol.%. The cathode flow is calculated in equation (1) by using nitrogen as reference gas, neglecting the small nitrogen loss by permeation. To normalize the helium permeate flux, $\dot{V}_{He}$ is divided by the inlet helium concentration.

$$\dot{V}_{He} = c_{He} \cdot \frac{c_{N_2}^o}{c_{N_2}} \cdot \dot{V} \cdot \frac{1}{c_{He}^o} \cdot \frac{1}{A} \qquad (1)$$

The increase of the helium permeate flux within two local gas sampling ports is plotted for each segment in Fig. 3B. The permeate flux of configuration A (pure diffusive gas transport at 140 kPa) is upscaled with a factor of 160/140 which gives the diffusive permeate flux at 160 kPa. The permeate flux of configuration B is subtracted from the upscaled permeate flux of configuration A resulting in the pure convective permeate flux (Fig. 3C). As expected, the convective gas transport is zero for new membranes. Both, the diffusive and convective permeate flux are expressed in terms of milliliter per second and square meter active area, where milliliter is referred to the standard condition at 25 °C and 101.3 kPa. The diffusive permeate flux is analyzed at an inlet anode pressure of 140 kPa and the convective permeate flux at 160 kPa with a pressure gradient between anode and cathode of about 10 kPa. Since the fuel cell is operated in counterflow configuration and the pressure gradients within the channel are typically 1.0 kPa and 3.5 kPa at the anode and cathode, respectively, the actual pressure gradient between anode and cathode may vary between 6.5 and 11 kPa. This is equal in all measurements, so the relative evolution of the convective gas crossover along the channel will not be affected.

Local changes in the diffusive and convective gas crossover were investigated in three different AST. The effect of chemical and mechanical membrane degradation on the gas separation was examined by applying OCV condition and relative humidity (RH) cycling. The combination of both was tested with a load cycling AST, which represents dynamic fuel cell operation. Experimental details

of the ASTs, which were adopted from DOE protocols [25], are given in Table 1.

2.2. Components

To test the effect of the GDE surface morphology on the durability of the membrane, a carbon cloth and a carbon paper gas diffusion electrode, named GDE "C" and "P", were used in the AST. The properties of the two GDEs are given in Table 2. The catalyst loading of GDE "P" is 0.1 mg(Pt) cm^{-2} and 0.4 mg(Pt) cm^{-2} for the anode and cathode, while it is 0.5 mg(Pt) cm^{-2} for both electrodes of GDE "C" (E-Tek Elat, A6 STDSI V2.1). The SEM images in Fig. 4A and B show the surfaces of the micro porous layer (MPL) of the pristine GDE "C" and "P". Both MPLs have cracks; the one on the paper based GDE "P" has a mean crack width of 5.4 ± 2.7 μm, which is less than in the one on the cloth (11.4 ± 6.9 μm). The crack surface coverage of GDE "P" is also 25% lower than for GDE "C". Unlike with the paper, carbon fibers pierce through the MPL of the cloth. Some of them break resulting in fiber endings, which are already present in the pristine GDE. Thus, they are not a result of the fuel cell operation. The GDEs were assembled with Nafion NR211 membranes, as this material shows a much better stability toward chemical degradation than Nafion 112/111 [16].

2.3. Experimental details

2.3.1. Experimental setup

A fuel cell of technical size with a linear flow field (28 channels), an active area of 200 cm^2 and channel dimensions of 0.8 × 0.5 × 400 mm has been equipped with fully heated gas extraction lines (Fig. 5). Details of the setup for local gas phase analysis were described previously [16,26]. Flow field plates are machined from PVDF bonded carbon plates (Sigracet BMA5, SGL Carbon). 12 μm thick Mylar foils (DuPont) are used as sub-gaskets outside the active cell area. Cell compression is adjusted by Teflon spacers to compress the GDEs uniformly to 70% of their initial thickness. The cell is operated using the following standard conditions in all ASTs: 0.557 L min^{-1} hydrogen (99.999%) and 1.36 L min^{-1} air in counterflow configuration. When analyzing gas permeation, 10 vol.% helium (99.999%) is added to the anode gas stream. A bubbler humidification system provides a relative humidity of 35% at the cathode and anode inlets, except for RH cycling where oversaturated gases are used for the wet cycle part. The anode and cathode outlet pressure are 150 kPa, and a thermostat maintains the cell temperature at 80 °C by heating the end plates uniformly with a liquid.
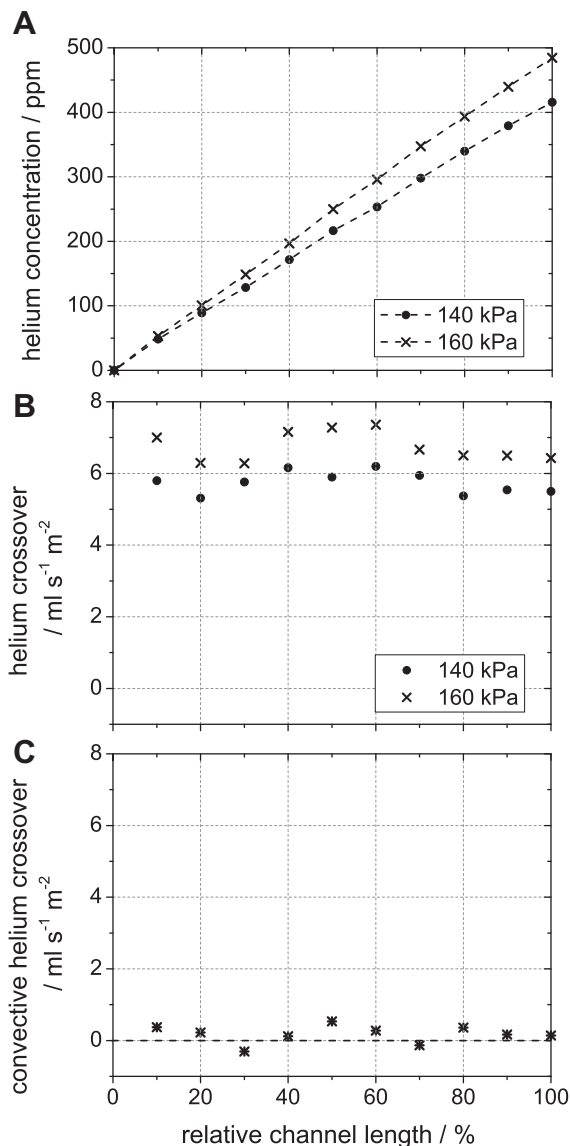
Fig. 3. A) Measured helium concentration in the center channel of the cathode. The cathode pressure is constant at 150 kPa, while the anode pressure is 140 or 160 kPa, respectively. B) The diffusive and total helium crossover are calculated from the derivative of the measured values at 140 and 160 kPa. C) The convective helium crossover is calculated by combining both data sets of B) where the diffusive helium crossover at 140 kPa is linearly extrapolated to the conditions at 160 kPa and then subtracted from the total crossover.

2.3.2. Gas analysis hardware

11 Gas extracting ports are aligned along the center channel of the linear cell described above, and two integral gas sampling ports are installed in the gas in- and outlet. 30 μl min^{-1} of gas is

Table 1
Experimental set points of the three accelerated stress tests adopted from the DOE protocols.

	OCV	RH cycling	Load cycling
Current density/mA cm^{-2}	0 (H$_2$/air)	0 (N$_2$/N$_2$)	0–300
Relative humidity/%	35	0–130	35
# Cycles	None	7500	30,000
Cycle holding time/s	None	120/120	30/30
Operating hours	500	500	500

Table 2
Properties of GDE "C" and "P".

	GDE "C"	GDE "P"
Base material	Carbon fiber woven cloth	Carbon fiber paper
Thickness/μm	250	200
Crack surface area coverage[a]/%	15.9 (±1.0)	12.0 (±1.8)
Mean crack width[a]/μm	11.4 (±6.9)	5.4 (±2.7)
MPL	Yes	Yes
Catalyst loading/mg cm^{-2}	0.5	0.1/0.4

[a] Optical evaluation from SEM images.

extracted from the channel and analyzed using a quadrupole mass spectrometer (Pfeiffer Prisma 200M1) with a lowest detection limit of 5 ppm for helium with a standard deviation of less than 1 ppm. Since the gas extraction volume is very low during the analysis, the gas flux and gas distribution are not expected to be influenced by the measurement [16]. Gas analysis is carried out at fuel cell standard condition without applying a load, except for RH cycling, where a nitrogen flow with a relative humidity of 35% is used on anode and cathode during gas analysis.

2.3.3. X-ray tomographic microscopy (XTM)

XTM allows for the nondestructive analysis of membrane samples, i.e. no preparation of samples by cutting or breaking of the membrane is required, which could induce artifacts, as it is the case for other microscopy techniques (visible light or electrons). Samples of the MEA were analyzed post mortem with XTM at the TOMCAT beamline of the Swiss Light Source. To find raw defects in larger membrane areas a number (8−10) of samples, 2 × 10 mm in size, were cut out of the MEA with a surgical knife, stored under air at room temperature and analyzed with a monochromatic X-ray beam of 13.5 keV at a pixel size of 0.74 × 0.74 μm^2 without binning [27]. Gray scale images were segmented manually by thresholding to produce clear 3D views of the actual samples.

2.3.4. Scanning electron microscopy (SEM)

SEM was employed to analyze the surface of the GDE. Small samples were cut out of the pristine GDE with a surgical knife and analyzed by SEM (FE-SEM Ultra 55, Carl Zeiss) at an acceleration voltage of 5 kV.

2.3.5. Fluoride emission rate (FER)

Effluent water was collected from the PEFC every 24 h, and the fluoride concentration was analyzed with ion chromatography (Compact IC plus with a Metrosep A Supp 5 150/4.0 column, Metrohm). The sensitivity at 10 ppb is less than 1 ppb with a standard deviation of less than 10%. The background fluoride concentration of the exhaust water is 70−130 ppb when the fuel cell is purged with fully humidified nitrogen at 80 °C. The virtual fluoride emission rate (FER) is 0−20 ng(F) cm^{-2} h^{-1} for the applied flow settings and inlet humidities from 0 to 100%. The BMA5 flow field plates emit fluoride, probably originating from PVDF, which may decompose partly during the production process of the material.

3. Results and discussion

The effect of chemical and mechanical membrane degradation on the gas separation is investigated by local gas permeation analysis. Dosing 10 vol.% helium to the anode gas at different pressure gradients of anode and cathode allows for *in situ*
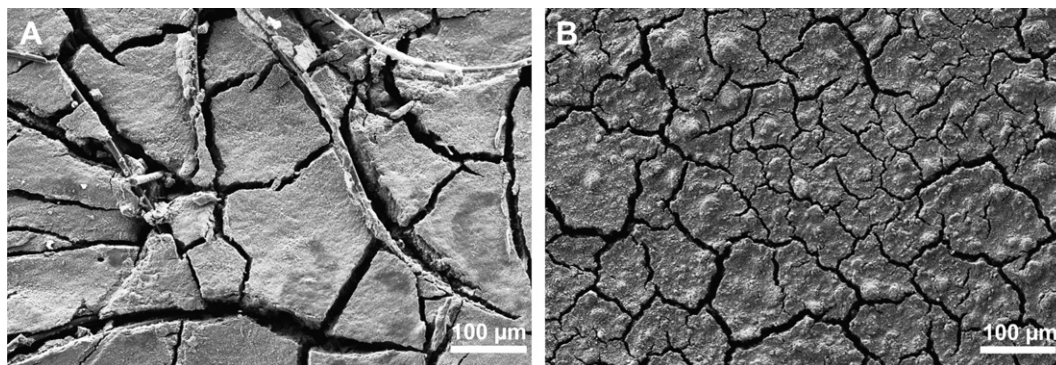
Fig. 4. *Ex situ* scanning electron microscopy images of pristine GDE surfaces. A) GDE cloth; carbon fibers of the GDE pierce through the MPL. B) GDE paper; cracks are present, but no carbon fibers.

analysis of the diffusive and convective gas transport across the membrane, from which membrane thinning and pinhole formation can be deduced. Inhomogeneous membrane degradation is further characterized by *ex situ* XTM, local water vapor analysis and *ex situ* SEM. MEAs with two different types of GDE are aged at OCV, relative humidity (RH) cycling and load cycling in order to accelerate chemical and mechanical degradation and their combination.

Figs. 6 and 7 show the local diffusive and convective helium crossover for MEA "C" (A, B, C) and MEA "P" (D, E). The initial *diffusive* helium crossover of new membranes (0 h) is about 5 ml s^{-1} m^{-2} and homogeneous along the channel. This is characteristic for new and intact membranes and corresponds to a mean hydrogen crossover of 2 ml s^{-1} m^{-2} assuming a permeability ratio of 2.5 for helium and hydrogen at 80 °C [16]. The hydrogen permeation is in agreement with data reported in the literature [28]. The initial *convective* helium crossover of new membranes fluctuates around zero. As expected, there are no detectable pinholes. In the following three subsections results of the three different accelerated stress tests (AST) are discussed in detail.

3.1. OCV AST

PFSA membranes decompose chemically by a radical attack mechanism, which is unzipping the polymer backbone from remaining carboxyl end groups as e.g. described by LaConti et al. [5]. This mechanism mainly causes membrane thinning, increased gas crossover and voltage loss [29]. Protecting the polymer backbone by fluorinating the carboxyl end groups reduces the chemical

degradation rate. This is observed when the Nafion 2xx series materials (end-groups fluorinated) are compared to the 1xx series membranes. Chemical degradation can be investigated with OCV accelerated stress tests, such as proposed by the DOE [25]. With this AST no humidity fluctuations, responsible for mechanical degradation, are induced as shown in Fig. 8A, where the local online water vapor analysis does not show any RH fluctuations.

The local and temporal evolution of the diffusive and convective gas permeation of MEA "C" are illustrated in Figs. 6A and 7A. Neither the helium diffusion nor the membrane thickness, measured with SEM, changed after the 500 h AST. The FER, an indicator used for chemical degradation and polymer decomposition [5], is on average 10.4 ng(F) cm^{-2} h^{-1} in this test, which is within the background obtained when operating the cell with nitrogen. Thus, a measurable chemical degradation of the membrane polymer has not been detected with the applied analysis methods. In spite, the convective gas crossover increases locally up to 9 ml s^{-1} m^{-2} in the cathode *outlet region* at 70% of channel length, which corresponds to an increase of 10 μl s^{-1} m^{-2} h^{-1}. An initial defect may accelerate chemical polymer decomposition locally due to the elevated gas crossover, which increases the radical formation rate. However, this may not be equally the case for all defects. Preliminary OCV experiments with Nafion 112 show that the convective helium permeation increases nonuniformly at statistically scattered spots [16].

In summary, no membrane thinning is observed for Nafion 211, which would be the commonly expected effect when focusing on chemical membrane degradation in a 500 h OCV AST [29]. However, the local convective gas crossover increases indicating the formation of pinholes.
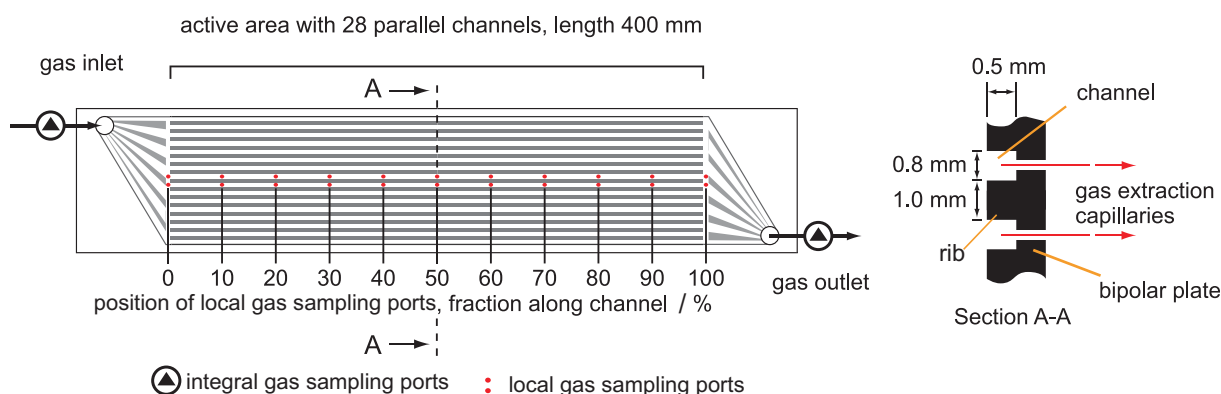

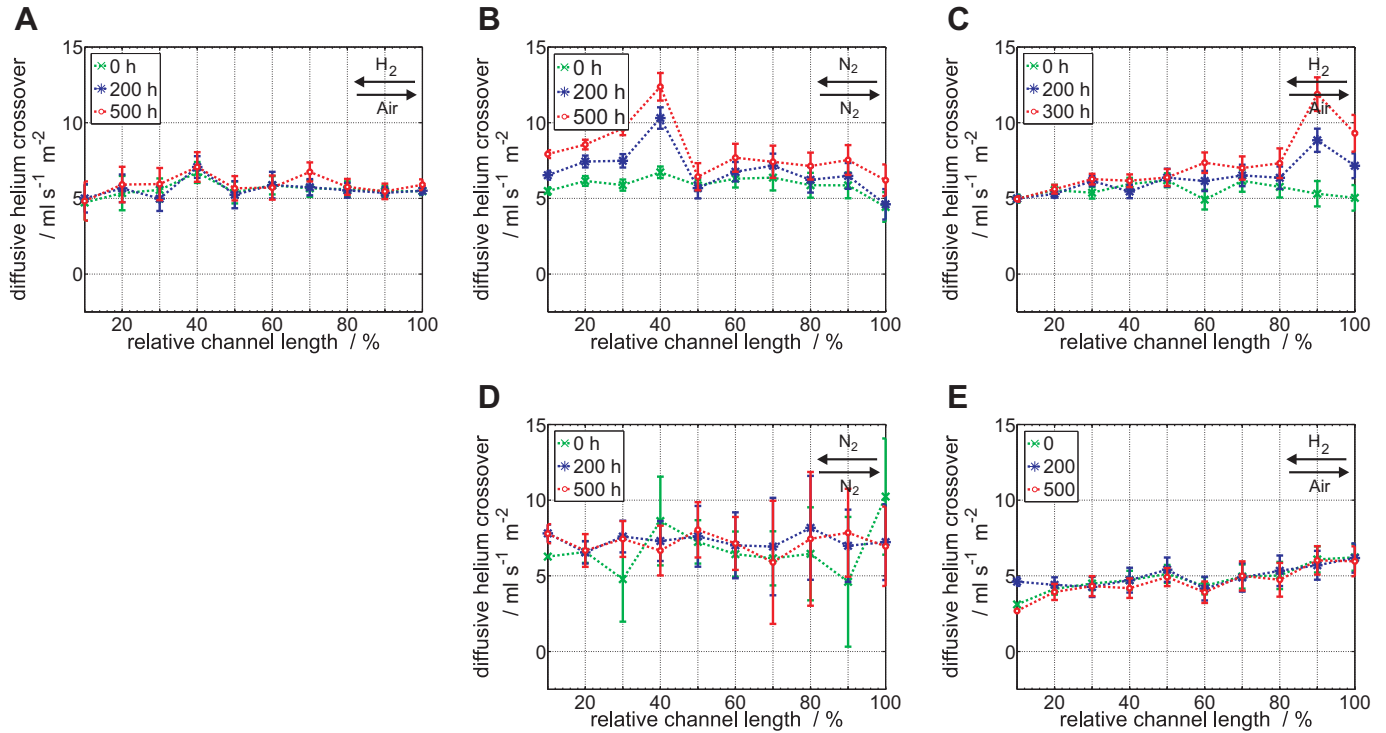**Fig. 5.** Schematic of cell instrumented for local gas analysis.

Fig. 6. The diffusive helium crossover as function of channel length for MEA "C" at A) OCV, B) RH cycling and C) load cycling and for MEA "P" at D) RH cycling and E) load cycling. The helium crossover is given in "ml" where "ml" refers to 25 °C and 101.3 kPa.

3.2. RH cycling AST

Fluctuations of the water content induce mechanical stress in the membrane through repeated swelling and shrinking. This process degrades the gas separation of the membrane by creeping, crack and pinhole formation [29]. To investigate these mechanical degradation processes, accelerated stress tests which only cycle the gas humidity are used. However, these tests may
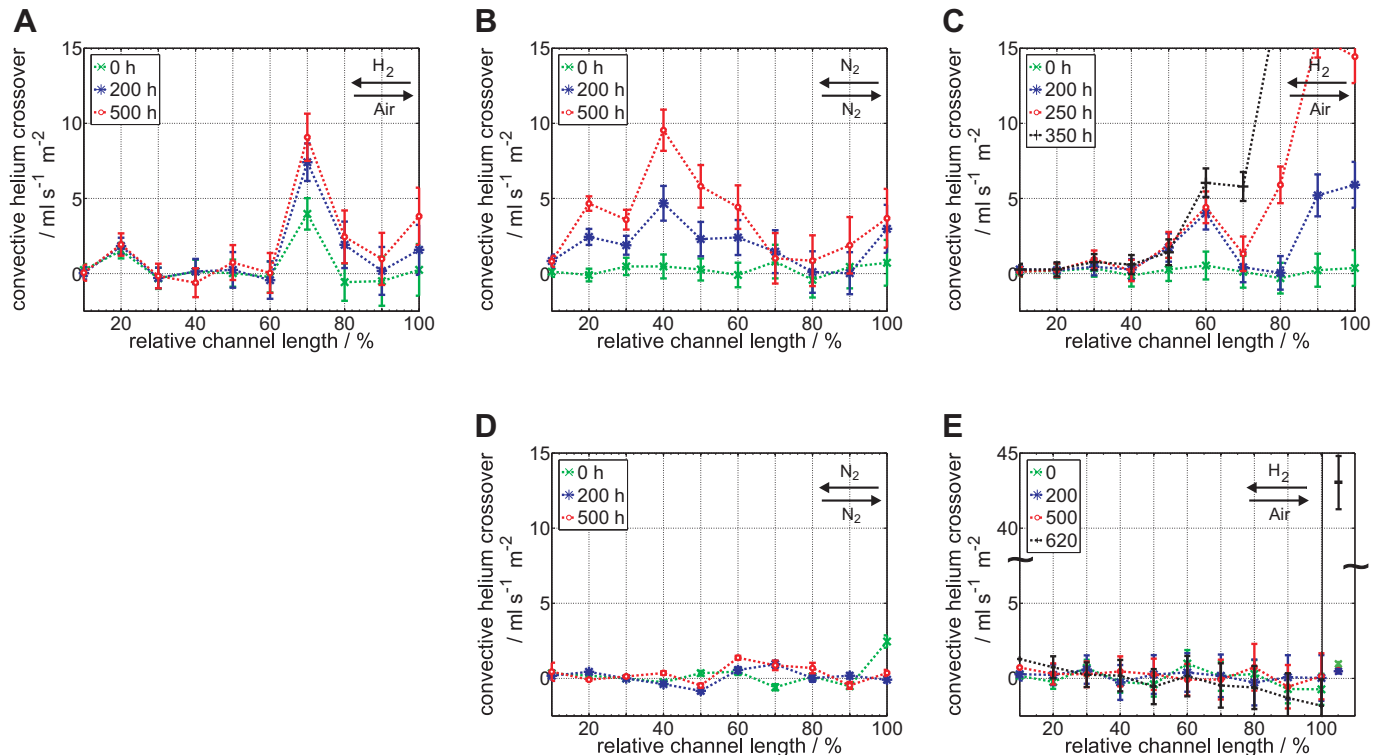

Fig. 7. The convective helium crossover as function of channel length for MEA "C" at A) OCV, B) RH cycling and C) load cycling and for MEA "P" at D) RH cycling and E) load cycling. The helium crossover is given in "ml" where "ml" refers to 25 °C and 101.3 kPa.
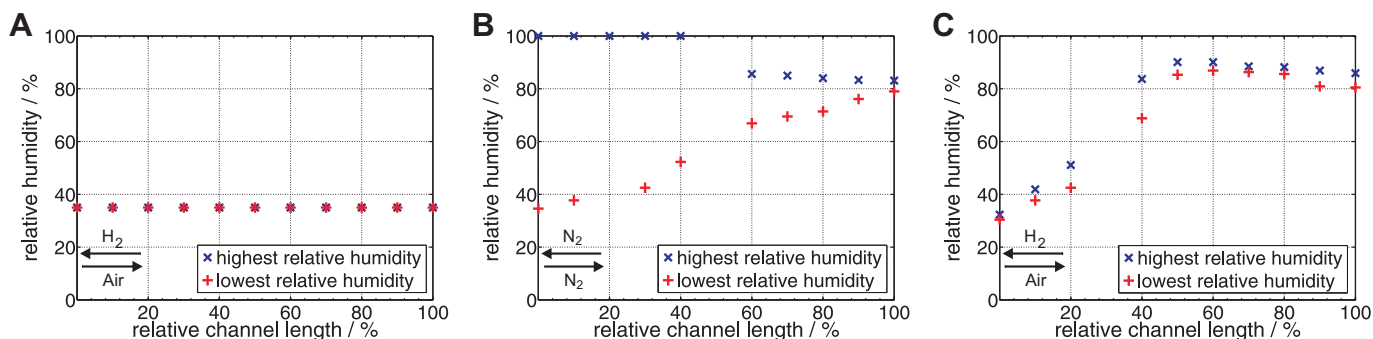
Fig. 8. *In situ* water vapor analysis in the center channel of the cathode. The minimum (red plus) and maximum (blue cross) relative humidities during the cycles are shown along the channel for A) OCV, B) RH cycling and C) load cycling. (For interpretation of the references to colour in this figure legend, the reader is referred to the web version of this article.)

induce inhomogeneous, transient humidity conditions in cells with a large active area, depending on the water storage capacity of the MEA and the cycling frequency. This calls for analysis of the local humidity fluctuations even when using standard protocols. Fig. 8B illustrates the RH fluctuations measured along the cathode channel of the cell. The RH cycling protocol has been adopted from the DOE protocol [25], with a dry (2 min) and wet (2 min) cycle with the inlet humidity changing between 0% and 130% (oversaturated gas). However, the control measurements show a minimum of only 34% and a maximum of 100% relative humidity at the cathode inlet. Water droplets, condensing in the MEA during the wet cycle, buffer the relative humidity in the dry cycle, which results in a maximum RH difference of only 66% in the cathode gas inlet. Due to the humidity buffering effect of the MEA, the RH fluctuation even decreases along the channel and almost disappears in the outlet region. So, the MEA acts as a buffer system and damps the humidity oscillations. Apparently, a cycling time of 2 min is not long enough to dry or humidify the cathode outlet region in this cell configuration completely. This leads to a nonuniform RH cycling amplitude along the channel. The effect of this nonuniform RH cycling on the membrane integrity is studied by analyzing the temporal and local evolution of both the diffusive and convective gas permeation. The AST is performed with two different MEA configurations to investigate the effect of the GDE surface roughness on the mechanical degradation rate of the membrane. GDE "C", based on a carbon fiber cloth, is compared to GDE "P", based on a carbon fiber paper, which has a smoother surface with less and narrower cracks in the MPL than GDE "C" (details see Table 2).

Fig. 6B and D show the local and temporal evolution of the diffusive and Fig. 7B and D of the convective gas permeation. The diffusive helium transport through MEA "C" increases with rates between 4 and 12 μl s^{-1} m^{-2} h^{-1} in the cathode inlet region (0–40%

of channel length) averaged over the 500 h test, while it does not change for MEA "P". The diffusive gas transport cannot only increase due to chemical membrane thinning, but also due to plastic deformation of the membrane, most likely induced by the irregularities of the GDE surface structure. Fig. 9A and B illustrate groove formation and membrane creeping in MEA "C". Grooves are formed in the polymer when sharp edges of MPL cracks exert a shear force on the polymer during membrane swelling. Likewise, the polymer counteracts the clamping pressure by creeping into MPL cracks; the larger the crack, the easier. Both processes cause local membrane thinning, which increases the diffusive gas transport through the membrane.

The gas diffusion through MEA "C" increases in the *inlet region*, caused by the larger humidity fluctuation and possibly by the high humidity, as water acts as plasticizer in the membrane material. Both, humidity fluctuations and a high membrane water content promote membrane creeping on the one hand due to the build-up of internal stress [23] and on the other hand by lowering the Young's modulus of Nafion at elevated water content [30]. The gas diffusion through MEA "P" does not increase, since plastic deformation of the membrane is less pronounced than for MEA "C" due to the smoother GDE surface with less and significantly smaller cracks. The smaller cracks, present on the surface of GDE "P", may only slow down plastic deformation and not eliminate it. Thus, it is not observed in the 500 h test.

A similar trend, as perceived for the diffusive crossover, is observed for the temporal and local convective crossover. The convective helium transport through MEA "C" increases with rates between 6 and 18 μl s^{-1} m^{-2} h^{-1} in the cathode *inlet region* (0 to 60% of channel length) averaged over the 500 h test, while it does not change for MEA "P". Carbon fiber endings pierce through the MPL of GDE "C" (see Fig. 4A) and can induce local stress by
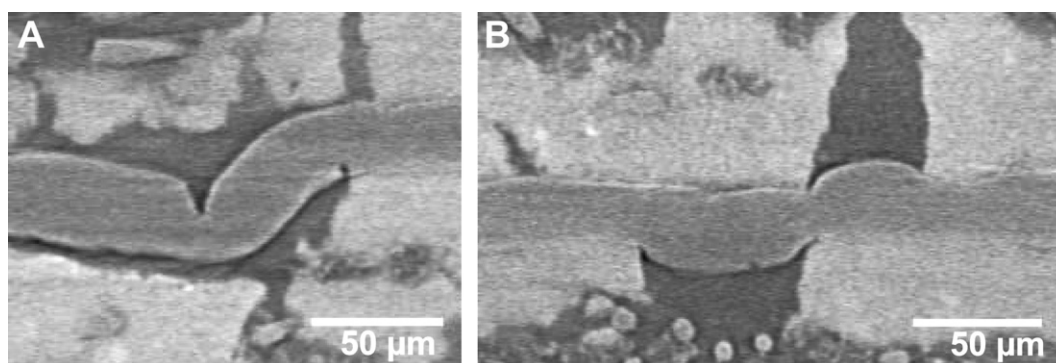

Fig. 9. *Ex situ*, post mortem X-ray tomographic microscopy cross-sections of degraded membranes. A) Illustrates a crack in the membrane and B) membrane creeping.
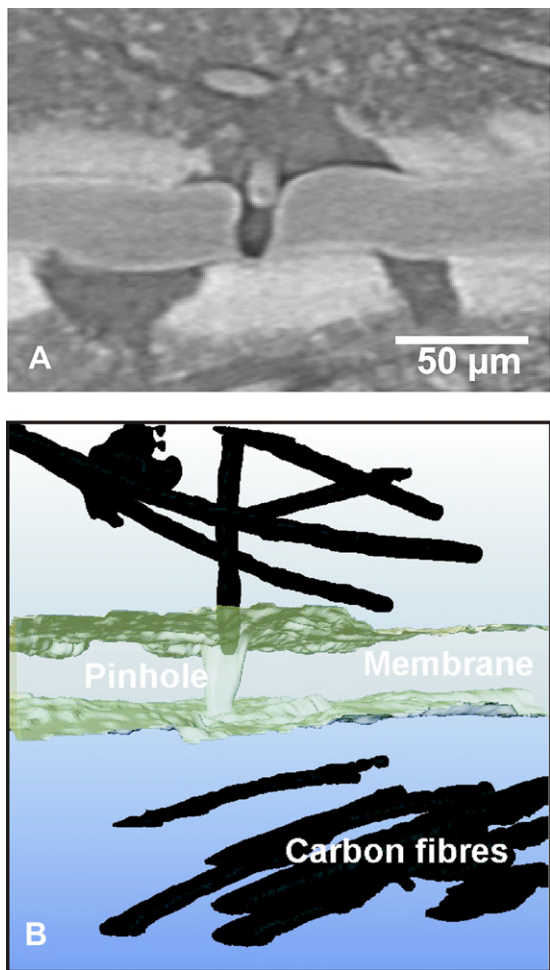
Fig. 10. *Ex situ* X-ray tomographic microscopy of a degraded MEA with a pinhole in the membrane. A) Cross-section, B) 3D visualization without the MPL.

penetrating into the membrane, which initiates pinhole formation. *Ex situ*, nondestructive, post mortem XTM analysis shows the presence of pinholes and carbon fiber endings next to these pinholes. Fig. 10A and B show a MEA cross-section as gray scale image and the corresponding segmented 3D structure of MEA "C" with a pinhole in the membrane, as typically found after applying RH cycling AST. The pinhole has a diameter between 4 and 13 μm, and a carbon fiber ending penetrates into the membrane in this case. Larger humidity fluctuations and possibly the high average humidity also promote pinhole formation in the cathode *inlet region* similar to membrane creeping.

At least one further mechanism for mechanical pinhole formation exists, since pinholes are also found in MEA "C" without fiber endings next to it. Sharp edges of MPL cracks intrude into the membrane during swelling and shrinking and exert shear forces on the polymer. This induces grooves in the membrane as depicted in Fig. 9A, which may further evolve to pinholes. Pinholes are not detected in MEA "P" within the 500 h test period, but mechanical pinhole formation may only be slowed down and not eliminated.

Summarizing, mechanical membrane degradation is caused and accelerated by the combined effects of the GDE surface morphology, large RH fluctuations in the gas channel and a high membrane humidification. Since the relative humidity and RH fluctuations are inhomogeneous along the channel, the diffusive and convective gas permeation also develop nonuniformly along the channel, i.e. the cell area.

3.3. Load cycling AST

This test is employed to investigate the combined effects of chemical and mechanical degradation processes on the membrane durability. The impact of the GDE surface properties is tested again using MEAs with GDE "C" and "P". During load cycling water is produced and accumulates along the channel, leading to a nonuniform water distribution as shown in Fig. 8C. Despite the alternation between OCV and load, the relative humidity increases almost without fluctuations from 35% to 90% along the cathode channel. The water storage capacity of the GDEs compensates for the fluctuating water production within the cycling time of 30 s.

The effects of this nonuniform water distribution and of the combined chemical and mechanical degradation processes on the membrane integrity are again studied by analyzing the temporal and local evolution of the diffusive (Fig. 6C and E) and convective (Fig. 7C and E) gas permeation. The diffusive helium transport through MEA "C" increases with rates between 11 and 18 μl s^{-1} m^{-2} h^{-1} in the cathode *outlet region* (90–100% of channel length). As observed in the RH cycling AST (Fig. 6B), a high humidity promotes plastic deformation of the membrane in the cathode outlet region, going along with an increasing gas diffusion. In MEA "P" the permeation does not increase during the 500 h test. Plastic deformation is weaker and not observed due to the smoother surface of GDE "P". Chemical decomposition of the membrane polymer is not observed by FER analysis. The mean FER of 8.2 ng cm^{-2} h^{-1} is within the background.

The convective helium crossover through MEA "C" increases with rates between 15 and 215 μl s^{-1} m^{-2} h^{-1} (78 μl s^{-1} m^{-2} h^{-1} on average) in the cathode *outlet region* (60–100% of channel length), while changes for MEA "P" are only observed in the integral outlet after 500 h (Fig. 7E; single markers on the right side), but not in the center channel. The gas crossover increases with a mean rate of 70 μl s^{-1} m^{-2} h^{-1} averaged over 620 h. If pinholes are not located in the center channel region, they are usually still detectable, since helium diffusion is fast among adjacent gas channels [16]. Thus, pinholes of MEA "P" are presumably located in the cathode outlet region of the outer channels, where the remaining residence time of the gas is too short to allow gas diffusing to the center channel.

The convective gas crossover probably increases in the cathode outlet region for the same reason as for the diffusive crossover. In addition, a high upstream hydrogen crossover may promote chemical polymer decomposition. The pressure gradient from

Table 3
Summary of the mean diffusive and convective helium crossover increase rate, where "μl" refers to 25 °C and 101.3 kPa.

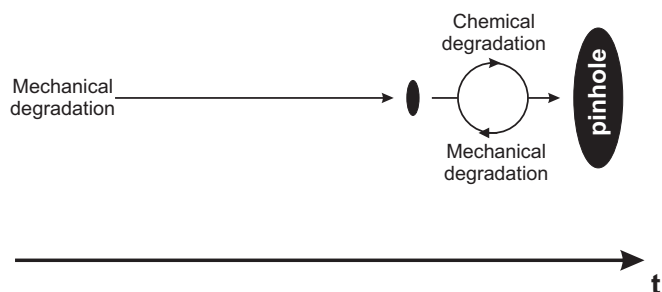|	GDE material	Diffusive helium crossover increase/μl s^{-1} m^{-2} h^{-1}	Convective helium crossover increase/μl s^{-1} m^{-2} h^{-1}	Relative channel length/%
OCV	GDE "C"	0	10	70–100
RH cycling	GDE "C"	4–12	6–18	0–50
	GDE "P"	0	0	
Load cycling	GDE "C"	11–18	15–215 (78 average)	60–100
	GDE "P"	0	70	Integral outlet

Fig. 11. Schematic drawing of the synergetic effect of chemical and mechanical membrane degradation for Nafion 211 due to pinhole formation.

anode to cathode and the hydrogen concentration are highest in the cathode outlet region in counterflow configuration.

The convective gas crossover increases much faster during load cycling (78 µl s^{-1} m^{-2} h^{-1} on average) than during RH cycling (6–18 µl s^{-1} m^{-2} h^{-1}) and OCV AST (10 µl s^{-1} m^{-2} h^{-1}) as summarized in Table 3. So, chemical and mechanical processes seem to have a synergetic effect with positive feedback on membrane degradation. As outlined by Huang et al. [12], the polymer looses its mechanical integrity partly when it decomposes chemically. Thus, pinholes and cracks will be formed faster by mechanical processes if some chemical degradation is present. The gas crossover through pinholes accelerates chemical polymer decomposition locally, which in turn enhances mechanical membrane degradation. As illustrated in Fig. 11, this loop accelerates pinhole growth and boosts the gas crossover (Fig. 7C). The severity is similar for both MEA "C" and "P", but the onset of the degradation loop is different. Pinholes are formed mechanically in MEA "C" within 200 h, but not until 500 h in MEA "P" due to the smoother surface roughness of GDE "P". So, the synergetic effect of chemical and mechanical degradation processes starts later for MEA "P".

Summarizing, chemical and mechanical processes induce a synergetic effect on membrane degradation, which accelerates the overall degradation rate. Pinhole formation is critical for the onset of the synergetic effect, which seems to be triggered by mechanical processes induced by the surface roughness of the GDE.

4. Conclusion

The effect of chemical and mechanical degradation on the gas separation of PEFC membranes is investigated locally in the early stage to identify trigger processes which lead to a nonuniform degradation. Using a tracer gas concept, gas permeation through MEAs is analyzed *in situ* and online in terms of diffusive and convective gas transport. Membrane thinning and pinhole formation are deduced from the temporal evolution of both. To test the influence of the GDE surface structure, two types of MEAs with different GDE surface morphology are used. Chemical, mechanical and the combined degradation of both are forced by OCV, relative humidity cycling and load cycling accelerated stress tests.

The initial gas crossover through the tested MEAs is given by the diffusive gas transport in Nafion 211 membranes, which increases due to mechanical but not due to chemical membrane thinning. Chemical decomposition of the tested Nafion 211 membranes is weak at OCV. Mechanical membrane thinning is induced by surface defects of the GDE exerting shear forces and causing plastic deformation of the polymer. This is accelerated by RH fluctuations in the gas channel and a high membrane water content. Due to the spatial nonuniformity of both, mechanical membrane thinning is inhomogeneous over the active cell area.

Primarily, pinhole formation accounts for the degradation of the gas separation of Nafion 211 membranes. Pinholes are formed mechanically by carbon fiber endings, originating from the GDE, or by MPL cracks, which exert local stress on the membrane. Once small pinholes (about 10 µm in diameter) are formed, the locally increasing gas crossover accelerates chemical decomposition of the polymer via the radical attack mechanism. The combination of chemical and mechanical degradation leads to a synergetic effect for membrane degradation, which accelerates pinhole growth and, in turn, boosts the gas permeation. The formation of small pinholes is crucial for the onset of the synergetic effect. Smooth GDE surfaces delay mechanical pinhole formation and extend the lifetime of the membrane. Areas with high relative humidity and RH fluctuations promote mechanical stress on the membrane resulting in an inhomogeneous degradation of the gas separation over the active cell area.

Acknowledgment

References

[1] P. Mock, S.A. Schmid, J. Power Sources 190 (2009) 133–140.
[2] J. van Dokkum, A. Dasinger, J. Power Sources 181 (2008) 378–381.
[3] J. Wu, X.Z. Yuan, J.J. Martin, H. Wang, J. Zhang, J. Shen, S. Wu, W. Merida, J. Power Sources 184 (2008) 104–119.
[4] W. Schmittinger, A. Vahidi, J. Power Sources 180 (2008) 1–14.
[5] A. La Conti, M. Hamdan, R. McDonald, in: Handbook of Fuel Cells - Fundamentals, Technology and Application, Wiley, Chichester, 2003, pp. 647–662.
[6] A. Collier, H. Wang, X. Zi Yuan, J. Zhang, D.P. Wilkinson, Int. J. Hydrogen Energy 31 (2006) 1838–1854.
[7] R. Borup, J. Meyers, B. Pivovar, Y.S. Kim, R. Mukundan, N. Garland, D. Myers, M. Wilson, F. Garzon, D. Wood, P. Zelenay, K. More, K. Stroh, T. Zawodzinski, J. Boncella, J.E. McGrath, M. Inaba, K. Miyatake, M. Hori, K. Ota, Z. Ogumi, S. Miyata, A. Nishikata, Z. Siroma, Y. Uchimoto, K. Yasuda, K. Kimijima, N. Iwashita, Chem. Rev. 107 (2007) 3904–3951.
[8] M. Inaba, in: Polymer Electrolyte Fuel Cell Durability, Springer, New York, 2009, pp. 57–69.
[9] H. Liu, H.A. Gasteiger, A. La Conti, J. Zhang, ECS Trans. 1 (2006) 283–293.
[10] N. Yousfi-Steiner, P. Mocotéguy, D. Candusso, D. Hissel, J. Power Sources 194 (2009) 130–145.
[11] J. Healy, C. Hayden, T. Xie, K. Olson, R. Waldo, M. Brundage, H. Gasteiger, J. Abbott, Fuel Cells 5 (2005) 302–308.
[12] X. Huang, K. Reifsnider, in: Modern Aspects of Electrochemistry, Springer, New York, 2010, pp. 1–43.
[13] V. Atrazhev, E. Timokhina, S.F. Burlatsky, V. Sultanov, T. Madden, M. Gummalla, ECS Trans. 6 (2008) 69–74.
[14] A. Panchenko, M.T.M. Koper, T.E. Shubina, S.J. Mitchell, E. Roduner, J. Electrochem. Soc. 151 (2004) A2016–A2027.
[15] S. Vengatesan, M.W. Fowler, X.-Z. Yuan, H. Wang, J. Power Sources 196 (2011) 5045–5052.
[16] G.A. Schuler, Diss. ETH No. 18883, Eidgenössische Technische Hochschule Zürich, Zürich, 2010.
[17] V. Stanic, M. Hoberecht Honolulu, in: Electrochemistry Society Conference (2004), p. 1891.
[18] S.R. Samms, S. Wasmus, R.F. Savinell, J. Electrochem. Soc. 143 (1996) 1498–1504.
[19] J. Yu, T. Matsuura, Y. Yoshikawa, M.N. Islam, M. Hori, Electrochem. Solid-State Lett. 8 (2005) A156–A158.
[22] B. Sompalli, B.A. Litteer, W. Gu, H.A. Gasteiger, J. Electrochem. Soc. 154 (2007) B1349–B1357.
[23] M.F. Serincan, U. Pasaogullari, J. Power Sources 196 (2011) 1303–1313.
[24] J. Stumper, R. Rahmani, F. Fuss, J. Power Sources 195 (2010) 4928–4934.
[25] US Department of Energy, United States, 2007.
[26] G. Schuler, A. Wokaun, F. Büchi, J. Power Sources 195 (2010) 1647–1656.
[27] F. Marone, C. Hintermüller, S. McDonald, R. Abela, G. Mikuljan, A. Isenegger, M. Stampanoni, J. Phys. 186 (2009) 012042.
[28] S. Takaichi, H. Uchida, M. Watanabe, Electrochem. Commun. 9 (2007) 1975–1979.
[29] S. Zhang, X. Yuan, H. Wang, W. Mérida, H. Zhu, J. Shen, S. Wu, J. Zhang, Int. J. Hydrogen Energy 34 (2009) 388–404.
[30] E. Roberti, G. Carlotti, S. Cinelli, G. Onori, A. Donnadio, R. Narducci, M. Casciola, M. Sganappa, J. Power Sources 195 (2010) 7761–7764.